Food Chemistry: X 22 (2024) 101434

Contents lists available at ScienceDirect

Food Chemistry: X

journal homepage: www.sciencedirect.com/journal/food-chemistry-x

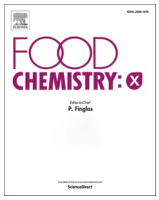

Fabrication of immobilized lipases from *Candida rugosa* on hierarchical mesoporous silica for enzymatic enrichment of ω-3 polyunsaturated fatty acids by selective hydrolysis

Zhe Dong, Jun Jin, Wei Wei, Xiaosan Wang, Gangcheng Wu, Xingguo Wang, Qingzhe Jin *

State Key Lab of Food Science and Resources, School of Food Science and Technology, Jiangnan University, Wuxi 214122, China

ARTICLE INFO

Keywords:
Omega-3 polyunsaturated fatty acids
Immobilization of lipase
Hollow silica microsphere
Hydrolysis

ABSTRACT

In this study, lipase from *Candida rugosa was* immobilized on hydrophobic hierarchical porous hollow silica microsphere (HPHSM-C3) via adsorption. The prepared biocatalyst HPHSM-C3@CRL exhibited higher activity, thermal and pH stability. HPHSM-C3@CRL remained 70.2% of initial activity after 30 days of storage at 24 °C and 50.4% of initial activity after 10 cycles. Moreover, HPHSM-C3@CRL was utilized in enzymatic enrichment of omega-3 polyunsaturated fatty acids (ω-3 PUFAs) in glycerides, achieving ω-3 PUFAs content of 53.42% with the hydrolysis rate of 48.78% under optimal condition. The K_m and V_{max} value of HPHSM-C3@CRL was 42.2% lower and 63.5% higher than those of CRL, respectively. The 3D structure analysis of CRL, substrates and pore structure of HPHSM-C3 suggested that the hierarchical pore improved activity and selectivity of immobilized lipase. This result demonstrated that HPHSM-C3@CRL may be an effective biocatalyst for the enzymatic enrichment of ω-3 PUFAs in food industries.

1. Introduction

Omega-3 polyunsaturated fatty acids (ω-3 PUFAs) play critical roles in anti-inflammatory, inhibition of cancer cells and cardiovascular disease (Carlson, Fallon, Kalish, Gura, & Puder, 2013; Fletcher et al., 2021; Hong et al., 2022). These biological functions are highly associated with the present form and content of ω-3 PUFAs in targeted products. Typically, ω-3 PUFAs are primarily in the form of glycerides, free fatty acids, and ethyl esters. The form in glycerides has attracted increasing concerns due to moderately higher oxidative stability and better bioavailability in digestion and absorption (Balasubramanian Ganesan & Donald, 2014; Moreno-Perez, Luna, Señorans, Guisan, & Fernandez-Lorente, 2015). Meanwhile, the predominant form of ω-3 PUFAs exists as glycerides in nature. In this context, ω-3 PUFAs in form of glycerides are of great value and interest.

The content of ω-3 PUFAs in nature are rather low, comprising about 30% of total fatty acids (Moreno-Perez et al., 2015). The concentration of ω-3 PUFAs rich in glycerides has been increasingly studied, especially focusing on enzymatic method due to mild conditions, energy-saving and low cost (Liu & Dave, 2022). For example, He et al., prepared monoacylglycerols (MAGs) rich in ω-3 PUFAs by enzymatic ethanolysis of sardine oil (He et al., 2017). By enzymatic hydrolysis of tuna oil, the ω-3 PUFAs content in glycerides was raised from 34.30% to 57.7%, and a second hydrolysis further increased the content to 68.94% (Chen et al., 2023; Yang et al., 2020). However, free lipase encounter difficulties in high price, limited thermal stability, and poor reusability. Enzyme immobilization could overcome these drawbacks and efficiently improve lipase activity and even selectivity (Ghiaci, Aghaei, Soleimanian, & Sedaghat, 2009a, 2009b; Sedaghat, Ghiaci, Aghaei, & Soleimanian-Zad, 2009). There have been reports about commercial immobilized lipase utilized in concentration of ω-3 PUFAs. Bispo. et al. used Lipozyme RM IM to enrich ω-3 PUFAs in glycerides at reaction temperature of 55 °C (Bispo, Batista, Bernardino, & Bandarra, 2014). Miranda et al. prepared the diacylglycerols (DAGs) rich in ω-3 PUFAs with Novozym 435 at 60 °C (Miranda, Baeza-Jiménez, Noriega-Rodríguez, García, & Otero, 2013). However, the risk of ω-3 PUFAs oxidation was highlighted when subjected to the high temperature and long-time incubation in these cases. Previously, our group demonstrated lipase from *Candida rugosa* (CRL) achieved the higher enrichment efficiency among six commercial lipases in selective hydrolysis of tuna oil (Yang et al., 2020). Meanwhile, several studies verified that CRL had highest preferences in hydrolysis in molecule level (Chen et al., 2019; Okada & Morrissey, 2007). However, there was little knowledge about the application of immobilized lipase in concentration of ω-3 PUFAs in

* Corresponding author.
E-mail address: jqzwx12@163.com (Q. Jin).

https://doi.org/10.1016/j.fochx.2024.101434
Received 5 January 2024; Received in revised form 28 April 2024; Accepted 29 April 2024
Available online 10 May 2024

glycerides.

The ideal carriers with proper microenvironment have pivotal roles in activity of immobilized lipase (Aghaei, Ghavi, Hashemkhani, & Keshavarz, 2020; Mortazavi & Aghaei, 2020). Mesoporous silica has been employed in immobilization of lipase due to its biocompatibility, high surface area, facile surface functionalization, and robust thermal stability. Recently, several studies reported lipase immobilized on the mesoporous silica carriers with hierarchical pore structure achieved great performance (Giulio, Andr'es-Sanz, Marta, & Giuseppe, 2024; Morales et al., 2023; Sun et al., 2018). Lipase was accommodated on the larger pore and the small chemical molecules could circulate through smaller pore. Thus, hierarchical pore provides elaborate accommodation for enzyme, minimizing diffusion barriers and thus enhancing mass transport. Additionally, the precise pore structure could also control the transfer of substrate in different size, thus improving lipase activity and even selectivity (Parlett, Wilson, & Lee, 2013). Considering that unique bending chain of ω-3 PUFAs and lipase 3D structure, immobilization of CRL on hierarchical porous materials is a promising strategy to improve lipase activity in enzymatic concentration of ω-3 PUFAs.

This study aims to prepare an effective and selective immobilized lipase for the enzymatic enrichment of ω-3 PUFAs in glycerides. The targeted lipase from *Candida rugosa* was immobilized on prepared hierarchical porous hollow silica microsphere and modified with trimethoxy (propyl)silane (HPHSM-C3). The characterization of HPHSM-C3 and its immobilized lipase was performed. The immobilization parameters were optimized. The thermal and pH stability, recycle and storage ability were evaluated. Eventually, the resulting immobilized lipase was utilized in enzymatic enrichment of ω-3 PUFAs in glycerides. The comparative discussion was conducted on the conformational change of immobilized lipase. The effect of hierarchical pore structure on substrate transfer, as well as activity and selectivity of lipase was also explored. The immobilized CRL is expected to serve as efficient biocatalyst for the production of structured lipids.

2. Materials and methods

2.1. Materials

Trimethoxy (propyl)silane (98%), *p*-nitrophenylpalmitate (*p*-NPP) was purchased from Sigma-Aldrich (St. Louis, MO, USA). The other chemicals like sodium metasilicate nonahydrate, CTAB, toluene, ethanol and triethylamine were obtained from Sinopharm Chemical Reagent (Shanghai, China) with purity of 99%. The lipase powder named AY30 (lipase from *Candida rugosa*, CRL for short) was gained from Amano Enzyme, Inc. (Nagoya, Japan). The BCA kit for protein assay was acquired from Beyotime Biotechnology (Shanghai, China). Refined tuna oil was obtained from NovoSana Co., Ltd. (Jiangsu, China).

2.2. Preparation of HPHSM

A modified method was applied in preparation of HPHSM based on the reference reported (Wu et al., 2010). Typically, 19.6 g of CTAB and 23.2 g of sodium metasilicate nonahydrate were dissolved in 337 mL of water at 30 °C for 1 h until the mixture became clear. Then, 35 mL of ethyl acetate was added rapidly into mixture with stirring vigorously for 30 s with 600 rpm (cantilever electric mixer LC-ES-60SH, Lichen Corp., Shanghai, China). The mixture was subjected to stand for 5 h before aged for 48 h at 90 °C. Finally, the solid product was obtained with centrifugation, performing on CR21N (Hitachi Corporation, Tokyo, Japan) with 6000 g at 20 °C. The resultant materials were cleared three times with pure water and ethanol. To remove CTAB molecules, the resulting particles were redispersing in the solution containing 1 M HCl (3.5 mL) and ethanol (100 mL), which was heat to 80 °C for 8 h. The prepared HPHSM was functionalized with trimethoxy (propyl)silane. Two grams of HPHSM, 5 mM of trimethoxy (propyl)silane and 60 μL of triethylamine were redispersed in 200 mL of toluene in a Teflon-lined stainless-steel autoclave (110 °C) for 20 h. The products were obtained by centrifugation (6000 *g*, 15 min), and washed three times with toluene and ethanol, which was designated as HPHSM-C3. The precise information about characterization of HPHSM-C3 was shown in supporting information.

2.3. Immobilization of lipase on HPHSM-C3

Immobilization of lipase was performed in a flask containing HPHSM-C3 and lipase solution (50 mM sodium phosphate buffer solution, pH 7.0, PBS). The initial protein concentration was determined using BCA Protein Assay Kit. Immobilization was conducted at 24 °C for 4 h using a water bath shaker. The bio-composite was separated by centrifugation (1000 *g*, 10 °C), which was then washed twice with PBS to remove any unabsorbed lipase. The concentration of residual enzyme solution was determined by BCA assay for immobilized protein calculation, as illustrated in Eq. (1):

$$IP = \frac{(C_0 - C_t)V}{m} \quad (1)$$

Where C_0 and C_t are the concentration of initial enzyme and residual enzyme solution (mg/mL), respectively. V stands for the volume of the loading lipase solution (mL), m denotes the mass of HPHSM-C3 (mg). The immobilized lipase was subjected to lyophilization and preserved at 4 °C, referred to as HPHSM-C3@CRL.

The effect of lipase concentration ranging from 0.5 to 3.0 mg/mL on the amount of immobilized protein was studied. Similarity, the effect of the immobilized time starting from 20 min to 180 min and support dosage from 0.05 mg to 0.15 mg in 10 mL lipase solution was also investigated.

2.4. Enzymatic hydrolysis assay for immobilized lipase

The immobilized lipase activity was evaluated through enzymatic hydrolysis of *p*-nitrophenyl palmitate (*p*-NPP) according to previous reference (Dong et al., 2024). The relative activity was calculated by dividing the remaining activity by the maximum activity. One unit of lipase activity (U) was described as the amount of biocatalyst that released 1 μmol of *p*-NP within a minute.

2.5. Stability and reusability of immobilized lipase

The thermal stability of the immobilized lipase was assessed by incubating it at temperatures between 30 °C -60 °C for 10 min, and then applied in hydrolysis of *p*-NPP. Similarly, the pH stability evaluation was carried out by incubating it at different pH buffer (5.0–9.0). The operational reusability of HPHSM-C3@CRL was evaluated through multiple consecutive cycles in the hydrolysis of *p*-NPP. The immobilized lipases were washed with PBS to eliminate any residual chemicals on the support surface after every cycle. The storage stability was evaluated by measuring hydrolysis activity after storing for several days (0, 1, 2, 4, 8, 10, 15, 30 days) at 24 °C (Aghaei et al., 2020).

2.6. Enzymatic enrichment of glycerides rich in ω-3 PUFAs

The enzymatic enrichment was performed on hydrolysis of tuna oil based on previous reference with some modifications (Yang et al., 2020). Briefly, the substrates tuna oil and phosphate buffer (50 mM, pH 7.0) were mixed with weight ratio of 1:1. The mixture was subjected to vigorous shaking for 30 s on a Vortex shaker (XW80A Vortex mixer, Shanghai) before 4 h incubation at 37 °C. The products were isolated by centrifugation (8000 *g*, 20 °C, 3 min). The upper oil phase was subjected to qualitative analysis by thin-layer chromatography (TLC) and high-performance liquid chromatography (HPLC) with refractive index detector (RID) as described below. The catalytic performance of HPHSM-C3@CRL was evaluated by content of ω-3 PUFAs in glycerides and

hydrolysis rate. The content of ω-3 PUFAs in glycerides was measured by analysis of fatty acids in glycerides fraction. Finally, the yield of ω-3 PUFAs was calculated as follows:

$$Yield = \frac{m_p \times \varphi_p}{m_r \times \varphi_r} \times 100\% \quad (2)$$

where m_p and m_r are the mass of glycerides product after the removal of FFAs and tuna oil. φ_p and φ_r are the content of ω-3 PUFAs in the tuna oil and glycerides product, respectively.

2.7. Analysis of glycerides rich in ω-3 PUFAs

2.7.1. HPLC analysis of hydrolysates

Hydrolysates detection was performed on HPLC-RID equipped with a Sepax HP-Silica column (4.6 mm × 250 mm × 5 μm, Sepax Technologies, Inc., Suzhou, China). The mobile phase was hexane, isopropanol and formic acid (15:1:0.003, *v/v/v*), following our previous study (Yang et al., 2020). All sample was dissolved in mobile phase with ratio of 1:500 (hydrolysates/mobile phase, *v/v*). The peaks of products, including TAGs, DAGs, MAGs and FFAs were aligned with the retention times of glycerides standards. The peak area percentage was calculated with respect to the total peak area. Hydrolysis rate was calculated by following Eq. (3) (Taiwo, Andrew, & Colin, 2014):

$$Hydrolysis\ rate\ (\%) = \frac{\alpha_r - \alpha_p}{\alpha_r} \times 100\% \quad (3)$$

where α_r and α_p are the peak area percentage of glycerides before and after hydrolysis, respectively.

2.7.2. Content of ω-3 PUFAs of hydrolysates

Firstly, the hydrolysates were separated by TLC (silica gel GF,UV-254 plate, thickness 2 mm, 10 cm × 20 cm) according to a previous report with some modifications (Jiang et al., 2022). The hydrolysates (20 mg) were dissolved in diethyl ether (150 μL) and then spotted onto TLC plate. The plate was placed in a TLC tank containing the developing solvent of *n*-hexane: diethyl ether: acetic acid (80:20:1, v/v/v). Meanwhile, the TAG, DAG, MAG and FFA standards were spotted and run in parallel with the samples as a site indicator. The developed plates were visualized in a tank filled with iodine vapor. Secondly, the corresponding bands were scraped off and the glycerides was extracted from bands

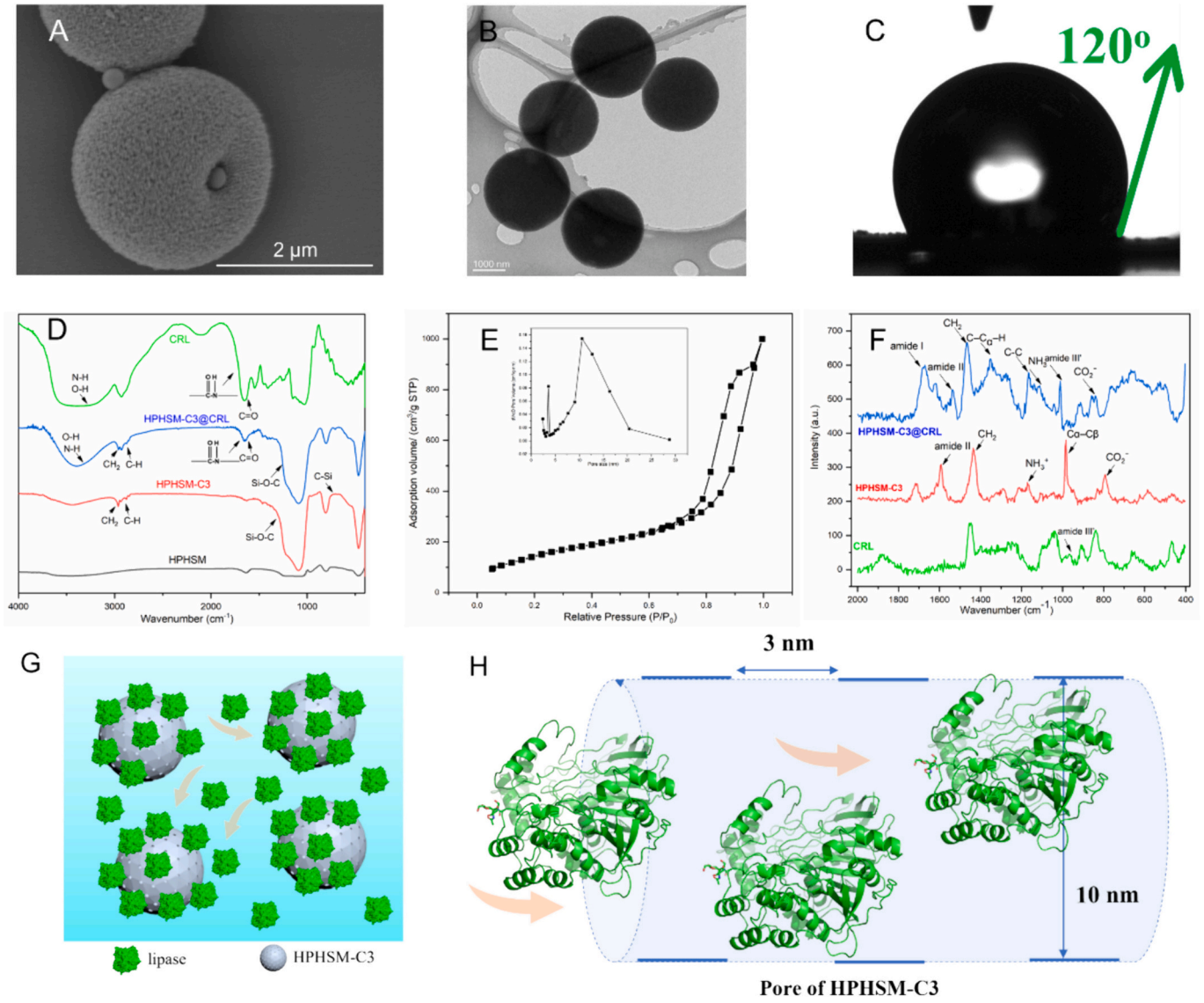

Fig. 1. SEM image (A) and TEM image (B) of HPHSM-C3; (C) Water contact angel of HPHSM-C3; (D) FT-IR spectra of CRL, HPHSM-C3 and HPHSM-C3@CRL; (E) N_2 adsorption−desorption isotherm and pore size distribution curve of HPHSM-C3(inset in (E)); (F) Raman spectra of HPHSM-C3, CRL, HPHSM-C3@CRL in the range of 400–2000 cm^{-1}.

with diethyl ether. After removal of the diethyl ether, the extracted glycerides and fatty acids were subjected to fatty acid composition analysis. Finally, the fatty acid in the glycerides fraction was converted into corresponding methyl esters via methyl- esterification reaction. The qualitative and quantitative analysis of fatty acid composition was performed by gas chromatography according to our previous study (Yang et al., 2020). All experiments were performed in triplicate.

3. Results and discussion

3.1. Characterization of HPHSM-C3 and HPHSM-C3@CRL

Fig. 1A-B displays the morphological characteristics and size of HPHSM-C3. The uniform surface morphology and hollow structure with around 2 μm in diameter were observed. The ordered pore distribution and fluffy surface contributed to lipase accommodation and mass transport. Previous studies have reported that hydrophobic support contribute to hyperactivation of lipases (Rodrigues et al., 2019). In this work, the carrier was modified with trimethoxy (propyl)silane. The water contact angle increased to 120° after functionalization, confirming the hydrophobicity of HPHSM-C3 (Fig. 1C). The prepared HPHSM-C3 exhibited two distinct characteristic absorption peaks at 2850 cm^{-1} and 2960 cm^{-1} compared to HPHSM in the FT-IR spectra (Fig. 1D), which corresponded to the symmetrical stretching vibration of -CH_2 and stretching vibration of -CH_3, respectively (Dong et al., 2019). It verified the successful chemical modification of HPHSM by trimethoxy (propyl) silane. Moreover, the pore parameters were listed in Table S1. The N_2 adsorption-desorption isotherms of HPHSM-C3 (Fig. 1E) exhibited a type IV isotherm. The large and clear H_1 hysteresis loop confirmed the relatively uniform pore distribution. The total pore volume was 1.6 cm^3/g, and the BET specific surface area was 559.1 m^2/g, indicating a high porosity of the HPHSM-C3. The pore size distribution, as shown in the inset of Fig. 1E, exhibited a characteristic hierarchically porous structure, comprising interconnected macropores (around 10 nm) and mesopores (3 nm) within the skeleton. Therefore, the lipase could be immobilized in macropores, while the substrates and products could transfer across mesopores, which was conductive to immobilization of lipase and catalytic process.

To certify immobilization of lipase on HPHSM-C3, the chemical structure was analyzed by FT-IR spectra and Raman spectra. FT-IR spectra in Fig. 1D revealed the characteristic peaks around 1600–1700 cm^{-1}, corresponding to stretching vibrations of C—H and C═O from Amide *I* bond, and C═N from amide II, as well as bending mode of NH single bond of CRL. The spectrum of HPHSM-C3@CRL showed six weak peaks in the region of 400–2000 cm^{-1} (Fig. 1F). Two bands at 1668 cm^{-1} and 1538 cm^{-1}can be assigned to the amino I and amino II mode from lipase, respectively. The band observed at 1538 cm^{-1} was associated to asymmetric bending of CH_3, CH_2 bending vibration and CH deformation motion (Chen et al., 2023). The weak bands at 945 cm^{-1}, 1598 cm^{-1} and 1720 cm^{-1} were attributed to N-Cα-C skeletal stretching of α-helix and the amide I and amide II mode. The bands between 1100 cm^{-1} and 1200 cm^{-1} were associated with NH_3 rocking vibration and NH_3^+ deformation vibration (Zhu, Zhu, Fan, & Wan, 2011). The bands observed at 1135 cm^{-1} 1178 cm^{-1} and 1187 cm^{-1} were assigned as rocking of NH_3^+ unit. The bands 900–1100 cm^{-1} in spectral region is characterized by C—C, C—N stretching vibrations. Two bands at 917 cm^{-1} and 1010 cm^{-1} were assigned to C-C-N stretching and C-O-H deformation of lipase (Adikwu Gowon, Roswanira Abdul, & Naji Arafat, 2021). The Raman spectra collectively confirmed immobilization of CRL on HPHSM-C3.

To better understanding of immobilization process, a scheme was provided in Fig. 1G and H. Firstly, the lipase was adsorbed on the surface via hydrophobic interaction. Then, the lipase molecules could go into the pore of HPHSM-C3 and accommodate in the pore. The successful immobilization on carrier was evidenced by appearance of green-fluorescence in confocal laser scanning microscope. Firstly, the lipase was labeled with fluorescein Isothiocyanate. This labeled lipase was immobilized on HPHSM-C3. This HPHSM-C3@CRL-labeled was visualized on CLSM. As shown in Fig. S1, the dyed lipase was present in the carriers, providing the evidence that lipase was accommodated on HPHSM-C3.

3.2. Optimization of immobilization of CRL on HPHSM-C3

Fig. 2A displayed the impact of initial lipase concentration on the quantity of loading protein and its relative activity. The effect of initial lipase concentration on amount immobilized protein and relative activity was illustrated in Fig. 2A. The immobilized protein elevated with the increasing lipase concentration, achieving the highest amount of 41.5 mg/g at lipase concentration of 2.5 mg/mL. Higher lipase concentration did not induce significant increase in amount on HPHSM-C3, suggesting that the HPHSM-C3 had achieved saturation of adsorption sites. Interestingly, the best relative activity of HPHSM-C3@CRL was gained at the lipase concentration of 2.0 mg/mL, while the amount of immobilize protein was 40.5 mg/g, which was lower than that of 2.5 mg/mL (41.5 mg/g). We inferred that the HPHSM-C3 was fully immobilized with lipase even causing aggregation at a concentration of 2.5 mg/mL, reducing the interaction between lipase and substrate. Accordingly, suitably lowering lipase concentration might not result in decrease in amount of immobilized lipase (from 41.5 mg/g to 40.3 mg/g), and even free up more space and providing more accessible active sites for substrate, and thus enhanced lipase activity (Machado et al., 2019). In summary, the optimal lipase concentration was 2.0 mg/mL.

The effect of support loading on immobilized protein and relative activity was investigated (Fig. 2B). The immobilized protein was dramatically decreased with the increasing of support dosage, while the relative activity exhibited a trend of initial increase followed by a subsequent decrease. The highest relative activity of HPHSM-C3@CRL was achieved at 0.1 g. This suggests that the increasing surface area or more accessible immobilization sites from increasing support dosage (higher than 0.1 g) did not significantly affect the adsorption process of HPHSM-C3 and its activity. The similar trend was observed with previous reports (Liu, Huang, Guo, Li, & Xiao, 2022). What really matters was immobilized protein on each HPHSM-C3 and its activity. In the fixed lipase concentration, the much higher amount of HPHSM-C3 was added in, the less amount of immobilized protein on each HPHSM-C3 particles was obtained. Therefore, considering the activity of HPHSM-C3@CRL, the support dosage was set as 0.1 g.

The effect of immobilization time was investigated (Fig. 2C), the immobilized protein was increased as immobilized time increased, reaching to a maximum loading amount of 37.5 mg/g at 2.5 h. In a recent report, it took 12 h for immobilization of lipase on chitosan/Fe_3O_4 magnetic nanocomposites, the similar long equilibrium time also occurred in the case of immobilization of CRL on $MgFe_2O_4$ nanoparticles (Morales et al., 2023; Zhao et al., 2022). The shorter equilibrium time implied that HPHSM-C3, with hierarchical pore sizes and larger surface areas, was a good candidate for adsorption immobilization of lipase. In conclusion, the immobilization time was 2.5 h in the following work.

3.3. Thermal, pH stability and reusability

The operational stability is a crucial criterion for the long-term and commercial application of immobilized lipase (Hamidreza, Atefeh, & Ameneh, 2021). Considering that the reaction temperature of lipase involved is relatively high, in general, the immobilized lipase demonstrates enhanced thermal stability relative to its free lipase (Aghaei, Mohammadbagheri, Hemasi, & Taghizadeh, 2022; Khozeymeh Nezhad & Aghaei, 2021). The effect of temperature on the relative activity of HPHSM-C3@CRL was investigated in the range of 30 °C to 60 °C (Fig. 2D). The free lipase achieved the highest activity at the temperature of 40 °C, and further rise in temperature led to the decrease in activity. However, HPHSM-C3@CRL exhibited superior activity than free

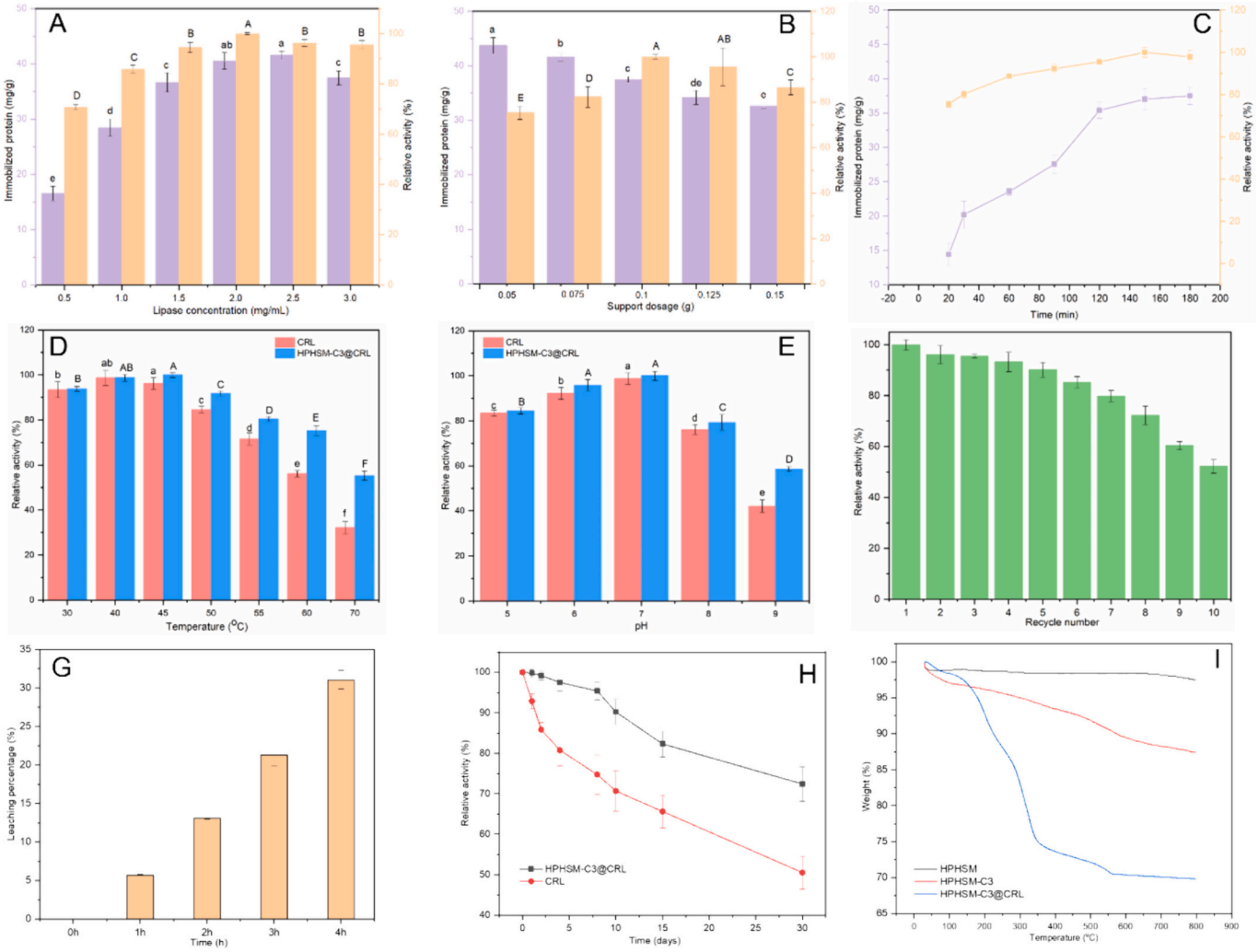

Fig. 2. Effect of lipase concentration (A), support dosage (B), incubation time (C) on amount of immobilized protein and relative activity of immobilized lipase; Effect of temperature stability (D), pH stability (E) and reusability (F) on the relative activity of free lipase and immobilized lipase; (G) The leaching percentage of HPHSM-C3@CRL incubation at different time; (H)The storage stability of CRL and HPHSM-C3@CRL; (I) TGA curves of HPHSM, HPHSM-C3 and HPHSM-C3@CRL.

lipase from 30 °C to 60 °C, and achieved highest activity at the temperature of 45 °C, implying that the HPHSM-C3 skeleton protected lipase from high temperature and improve its stability. It was reported that the free lipase might be agglomerated and deactivated in long-term incubation at high temperature (Aghaei et al., 2020). After the incubation at 70 °C, HPHSM-C3@CRL retained 50% of initial activity but the free lipase lost almost all the activity. The temperature and retained activity were higher than that of the recent report about immobilization of CRL on $MgFe_2O_4$ nanoparticles, which retained less than 10% at the temperature of 70 °C (Morales et al., 2023).

The optimal pH value of lipase might be changed after immobilization, and thus the influence of pH stability was studied. The highest activity of HPHSM-C3@CRL and CRL was obtained at pH 7 (Fig. 2E). HPHSM-C3@CRL showed higher activity than those of CRL in all pH value conditions. Remarkably, the activity of HPHSM-C3@CRL was 1.5 times higher than that of free lipase at pH of 9. The higher pH and temperature tolerance of HPHSM-C3@CRL might be attributed to the confinement of lipase within the hierarchical porous structures, which can improve the rigidity of lipase (Shahedi, Habibi, Yousefi, Brask, & Mohammadi, 2021). This result is in agreement with previous report showing that the increased stability of immobilized lipase could arise from improved conformational stability of lipase, lowered susceptibility to external environmental stimulus to protect from temperature and pH (Mostafavi, Poor, Habibi, Mohammadi, & Yousefi, 2024).

The recycle ability is a fundamental property for immobilized lipase in practical application. Recycle ability of HPHSM-C3@CRL was assessed for ten successive cycles (Fig. 2F). HPHSM-C3@CRL had superior reusability, retaining activity recovery of 55% until ten operational cycles. In addition, the recyclability of HPHSM-C3@CRL was higher than the previous report with the *Candida rugosa* lipase immobilized on chitosan-nanocellulose (retaining 44% after 8 times) (Nursyafiqah et al., 2018). The decreased activity might stem from the leaching of lipase from carriers. To test this assumption, the percentage of leaching was assessed by incubation at 24 °C for 1 h, 2 h and 4 h referred to the previous method (Aghaei et al., 2022). After centrifugation, the quantity of protein in the supernatant was determined. As shown in Fig. 2G, the HPHSM-C3@CRL showed increasing leaching, achieving the highest (32.8%) at 4 h. Thus, this result implied that binding affinity was weak by adsorption, and the covalent immobilization could be performed in the future.

The storage stability is also a critical property for successful employment in immobilized lipase. As shown in Fig. 2H, the relative activity of HPHSM-C3@CRL remained 70.2% activity, which was 20.5% higher than that of CRL after 30 days at 24 °C. Moreover, the decreasing rate in activity of HPHSM-C3@CRL was lower than that of CRL. It indicated that immobilization enhanced the storage ability of free lipase,

which might result from the protection of solid carriers (Aghaei et al., 2020).

TGA analysis was performed by HPHSM, HPHSM-C3 and HPHSM-C3@CRL (Fig. 2I). The weight loss of HPHSM-C3 accounted for 13.5%, resulting from the heating releasing of trimethoxy (propyl) silane. Interestingly, the weight loss of HPHSM-C3@CRL raised to 30.2%. In theory, the weight loss should be 3.6% according to loading amount of HPHSM-C3@CRL (37.5 mg/g). The exceptional weight loss might result from the other chemicals like carbohydrates and metal ions, which was immobilized on carriers together with lipase.

3.4. Enzymatic enrichment of glycerides rich in ω-3 PUFAs

3.4.1. Effect of enzyme loading on concentration of glycerides rich in ω-3 PUFAs

Given the significance of ω-3 PUFAs in functional lipids and healthy benefits, the enzymatic enrichment of ω-3 PUFAs was of great interest due to high selectivity and mild reaction condition. After the selective hydrolysis of saturated fatty acids (SFAs) and monounsaturated fatty acids (MUFAs) from TAGs, the ω-3 PUFAs could remain on glycerol skeleton (Fig. 3A). Thus, hydrolysis rate represents the hydrolytic activity of lipase, and the content of ω-3 PUFAs in glycerides is the indicator of biocatalyst activity and selectivity (Chen et al., 2019).

Fig. 3B-E showed the influence of enzyme loading and reaction time on the concentration performance of ω-3 PUFAs. As enzyme loading of CRL and HPHSM-C3@CRL increased from 2.5 U to 12.5 U, the hydrolysis rate was progressively increased, achieving 42.19% and 48.78% hydrolysis in 4 h, respectively (Fig. 3B). The hydrolysis rate of tuna oil did not significantly increase but even decrease with enzyme loadings higher than 12.5 U. It implied that the hydrolysis was in equilibrium, and HPHSM-C3@CRL or CRL at the concentration of 12.5 U provided sufficient active site for hydrolysis. Compared to free lipase CRL, HPHSM-C3@CRL achieved superior hydrolytic activity at each enzyme loading, suggesting that immobilization on HPHSM-C3 improve the hydrolytic activity of lipase. Similarity, the ω-3 PUFAs content in the glycerides successively increased with the enzyme loading increasing

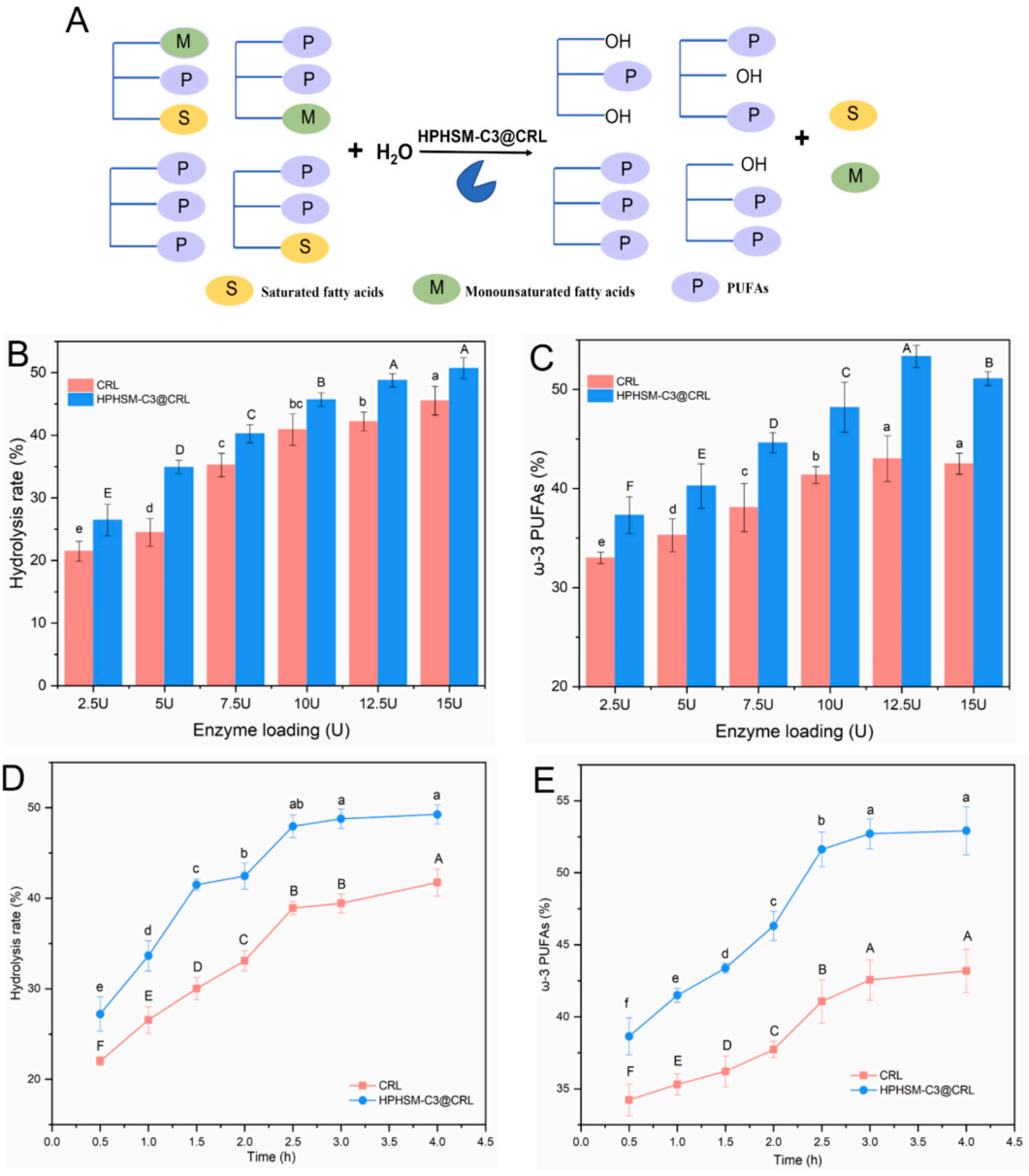

Fig. 3. (A) Lipase-mediated selective concentration of ω-3 PUFAs in glycerides; Effect of enzyme loading on the hydrolysis rate (B) and ω-3 PUFAs content (C); Effect of reaction time on the hydrolysis rate (D) and ω-3 PUFAs content (E).

from 2.5 U to 12.5 U (Fig. 3C). HPHSM-C3@CRL obtained highest ω-3 PUFAs content of 52.92% at loading dosage of 12.5 U. This content of ω-3 PUFAs was comparable with that of Yang et al., and Chen et al., reported (Chen, Liu, et al., 2023; Yang et al., 2020).

3.4.2. *Effect of pore size on lipase selectivity*

Interestingly, HPHSM-C3@CRL provided more higher ω-3 PUFAs content (44.63%) at enzyme loading of 10 U than that of free lipase (41.38%) at enzyme loading of 7.5 U, while they gained almost same hydrolysis rate (~40%), indicating that HPHSM-C3@CRL exhibited distinct selectivity during enzymatic hydrolysis. This selectivity might be related to unique molecular conformation of the double bonds in ω-3 PUFAs and physical microenvironment of HPHSM-C3. On the one hand, ω-3 PUFAs like DHA exhibited a curved conformation due to several double bonds in the chain, placing the terminal methyl group near the ester bonds, while non-ω-3 PUFAs like oleic acid and palmitic acid displayed a straight long chain, when they were in the stable state (Fig. 4A). The 3D structure size was analyzed with Multiwfn program (Lu & Chen, 2011). When three FFAs attached to the glycerol backbone, that was 1-oleoyl-2-docosahexaenoyl-3-palmitoylglycerol, which was the main substrate in this reaction. The 3D structure of this TAG was larger with the size of 4.3 nm × 1.6 nm × 1.2 nm, but the relative position of terminal methyl group and the ester bonds in DHA was remained (Fig. 4B). It was reported that here was a bent, L-shaped long internal tunnel (colored in pink), where the substrate binding site located (Fig. 4C) (Barriuso, Eugenia Vaquero, Prieto, & Jesus Martinez, 2016). Thus, the straight non-ω-3 PUFAs was more likely to bind and interact with catalytic active site. Owing to this steric hindrance effect, lipase active sites failed to break down the ester-linkages of these ω-3 PUFAs on the glycerol backbones, which coincidentally protected ω-3 PUFAs from lipase hydrolysis (Kahveci & Xu, 2011). On the other hand, compared with free lipase, HPHSM-C3@CRL possessed additional protection from support HPHSM-C3. From the BET pore distribution (Fig. 1F), HPHSM-C3 had the main pore size of 3 nm and 10 nm. Based on the calculation in Pymol script "draw protein dimensions" (version 2.5) (Calvo), the 3D size of CRL is 5.1 nm × 6.7 nm × 7.2 nm (Fig. 4C). As for the 3D structure of substrate, one of the most abundant TAG, 1-oleoyl-2-docosahexaenoyl-3-palmitoylglycerol was taken as an example. The length, width, and height of TAG is 4.3 nm × 1.6 nm × 1.2 nm (Fig. 4B). If the pore of HPHSM-C3 is like long cylinders with diameter of 10 nm, the TAG molecule preferred to going into the pore with the long chain of non-ω-3 PUFAs parallel with long cylinders (Fig. 4D). Furthermore, the ω-3 PUFAs were in the twisted shape but non-ω-3 PUFAs were with the straight linear shape. Thus, the non-ω-3 PUFAs were more likely to be cleaved by CRL and released to outside from pore of 3 nm. Hierarchically porous structure could further protect ω-3 PUFAs from lipase hydrolysis. Therefore, HPHSM-C3@CRL have higher selectivity on concentration of ω-3 PUFAs. Sun et al., has revealed the importance of hierarchically porous structure in augmenting the catalytic efficiency and selectivity of immobilized lipase, particular in transport of substrate and product (Sun, Aguila, Lan, & Ma, 2019).

3.4.3. *Effect of reaction time on concentration of glycerides rich in ω-3 PUFAs*

As shown in Fig. 3D, the hydrolysis rate of HPHSM-C3@CRL was much faster than that of free lipase, and reached the hydrolysis equilibrium with the shorter time. HPHSM-C3@CRL exhibited a hydrolysis rate of 47.94% after incubation for 2.5 h in 37 °C, while CRL showed 41.7%. The highest hydrolysis rate was observed in presence of HPHSM-C3@CRL at 4 h, achieving 48.78% hydrolysis rate. The ω-3 PUFAs content in glycerides was 42.5% at 2.5 h and little significant increase was observed with prolongation of time in presence of CRL (Fig. 3E). However, in the case of HPHSM-C3@CRL, ω-3 PUFAs content reached a maximum (52.8%) at 3 h. In the previous report, lipase AY400 achieved the ω-3 PUFAS content in the glycerides fraction of about 46% after enzymatic hydrolysis for 4 h (Yang et al., 2020). The improvement in hydrolytic activity of HPHSM-C3@CRL might result from the hydrophobic microenvironment of HPHSM-C3@CRL. Most lipases exhibit

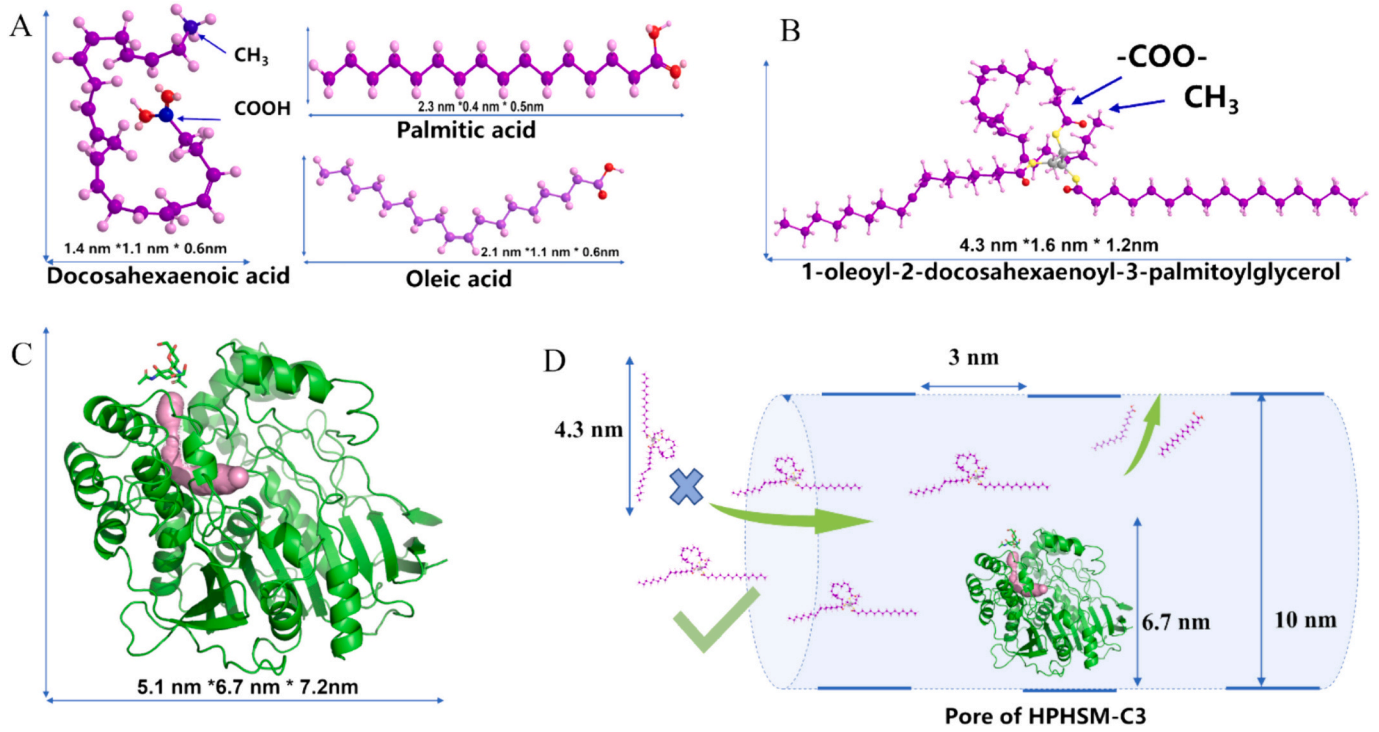

Fig. 4. (A) The length, width, and height of the molecules (A) oleic acid, docosahexaenoic acid and palmitic acid, (B) 1-oleoyl-2-docosahexaenoyl-3-palmitoylglycerol, which were analyzed by Multiwfn; (C) The length, width, and height of CRL by Pymol 2.5, the intramolecular tunnels highlighted in pink; (D) Schematic illustration of hydrolysis process that substrate entered pore of HPHSM-C3 and hydrolyzed by CRL, and then the released fatty acid could transfer via smaller pore in size of 3 nm. (For interpretation of the references to colour in this figure legend, the reader is referred to the web version of this article.)

interfacial activation, where an amphiphilic α-helical loop, named "lid", initially covering the active site in the native state (closed form), unfurls to roll back and provide full access to the catalytic triad (open form) in a hydrophobic medium, therefore bring about a significant increase in lipase activity (Sun et al., 2018). Immobilization of lipases on hydrophobic HPHSM-C3 is perceived to mimic the process of interfacial activation, promoting the opening of the amphiphilic lid and thus activating lipase (Rodrigues et al., 2019). The hydrophobic environment of HPHSM-C3 enables strong interactions between the hydrophobic groups surrounding the active site of lipase and the support surface. Meanwhile, the hydrophobic aperture could allow for interacting with inner hydrophobic part of lid and facilitating the lid opening of lipase, which accounts for the higher hydrolytic activity in selective hydrolysis of tuna oil.

To further demonstrate the difference in catalytic performance, the kinetic study was carried out using the Michaelis-Menten model (Fig. S2). The kinetic parameters were measured by determination of release of free acid, listed in Table 1. The K_m value was representative of binding affinity between substrates and enzyme. The lower K_m value means better binding affinity. The K_m value of HPHSM-C3@CRL was 42.2% lower than that of CRL. It indicated that HPHSM-C3@CRL have easier access for substrate, which might rise from the lid opening of lipase. The V_{max} value was 63.5% higher than that of CRL. Therefore, immobilization of CRL on HPHSM-C3 enhanced the lipase efficiency.

3.4.4. Reusability in concentration of glycerides rich in ω-3 PUFAs

No obvious variation in enzyme catalytic efficiency of HPHSM-C3@CRL was detected after being monitored for 5 cycles in selective hydrolysis (Fig. S3). HPHSM-C3@CRL still achieved hydrolysis rate of 38.56% and ω-3 PUFAs content of 44.83%, which was comparable to catalytic performance of free CRL in the first use. In enzymatic ethanolysis for enrichment of DHA in glycerides, Lipozyme TL IM retained 90.03% activity after 7 recycles (He et al., 2020). This result also indicated that the HPHSM-C3@CRL may be cost-effective and efficient biocatalyst with significant potential for applications in enzymatic synthesis of functional lipids and food industry.

3.5. Conformation analysis of immobilized lipase

As was described above, the hydrophobic microenvironment of HPHSM-C3@CRL could facilitate the opening of the lipase lid, thereby enhancing its catalytic efficiency. To test our hypothesis, FT-IR analysis of HPHSM-C3@CRL was performed to explore secondary conformation change of lipase before and after immobilization (Fig. 5). The amide I band (1600 cm^{-1}-1700 cm^{-1}) is recognized as the most sensitive spectral region of protein structural conformation, serving as a crucial indicator for determining secondary structure (Wang, Mo, Wu, Ma, & Wang, 2023). Therefore, the secondary derivative FT-IR spectra was obtained and evaluated based on the original spectra (Fig. 1D). Changes of CRL after immobilization on HPHSM-C3 were pronounced, as evidenced by the obvious differences in the position and the intensity of peaks in Fig. 5A. It indicated that the immobilization on HPHSM-C3 might affect the conformation and then improve the catalytic activity. This result was consistent with the abovementioned superior catalytic performance. To further clarify the structural transformation in detail, the quantitative and qualitative analysis of lipase secondary structure was calculated by curve fitting (Fig. 5B-C) and each content value was listed in Table S2. It seemed that some β-sheet structures of CRL were turned into β-turn structures after immobilization on HPHSM-C3. Meanwhile, there was little change in content of random coils but significant decrease in content of α-helix. Several studies on lysozyme (Vertegel, Siegel, & Dordick, 2004), lipase (Cao et al., 2020) and phospholipase A2 (Suladze, Cinar, Sperlich, & Winter, 2015) have revealed that the α-helix structures had a critical role in their activity. In this work, relative content of α-helix in HPHSM-C3@CRL decreased by 2.53%, which might be associated with movement and opening of α-helical lid. A previous study on crosslinked lipase reported that the decrease in relative content of α-helix had a positive effect on lipase activity (Cao et al., 2020).

Table 1
The kinetic parameters based on the Michaelis–Menten equation for CRL and HPHSM-C3@CRL.

Sample	K_m	V_{max} (mmol/min)	R^2
HPHSM-C3@CRL CRL	2.63	3.53	0.93
CRL	4.55	1.29	0.95

Reaction conditions: lipase loading: 12.5 U, ratio of tuna oil to PBS: 0.5–3.5 (the optimal ratio was 1), reaction time: 3 min, reaction temperature: 37 °C.

3.6. Fatty acid composition after selective hydrolysis by lipase

The triacylglycerols in tuna oil account for 99.34%. The primary fatty acids were DHA (24.25%) and palmitic acid (21.4%), followed by oleic acid (17.64%) and stearic acid (6.92%), as listed in Table S4. The ω-3 PUFAs, including DHA (22:6 ω-3), EPA (20:5 ω-3), and ALA (18:3 ω-3), comprised 32.24% of the total fatty acids. After selective hydrolysis by HPHSM-C3@CRL at 37 °C for 4 h, the hydrolysates contained TAGs (32.18%), FFAs (52.58%), DAGs (14.22%) and MAGs (1.03%), affording hydrolysis rate of 48.78% (Table S3). This hydrolysis rate was increased by 7.05% compared with that of free lipase (41.53%). Compared the fatty acid composition of TAGs in substrate and product (Table S4), as expected, the ω-3 PUFAs content increased from 32.24% to 53.42% in the presence of HPHSM-C3@CRL with the yield of 91.1%. However, the ω-3 PUFAs content in glycerides fraction obtained with CRL as a biocatalyst was only 43.19%, indicating that HPHSM-C3@CRL has an excellent catalytic performance in concentration of ω-3 PUFAs in glycerides. The yield reached to 85.05% in the first hydrolysis by CRL and then decreased to 71.64% in the second hydrolysis by *Candida antarctica* lipase A (CALA) in previous study (Chen, Liu, et al., 2023). The authors found that the selectivity was much higher than that of CRL in the second hydrolysis and the combination of two lipases achieved better enrichment performance. The strategy that immobilization of CALA could be considered in the future to gain higher ω-3 PUFAs content in glycerides.

4. Conclusion

The purpose of this study was to fabricate the immobilized lipase for enzymatic enrichment of ω-3 PUFAs in glycerides. Thus, lipase from *Candida rugosa* was immobilized on HPHSM-C3 via adsorption and the successful preparation was confirmed by advanced tools such SEM, FTIR and Raman. The prepared HPHSM-C3@CRL exhibited enhanced activity, thermal stability and pH stability compared with that of CRL. It remained 70.2% of initial activity after 30 days of storage at 24 °C and 50.4% of initial activity after 10 cycles. Specifically, the immobilized lipase achieved a ω-3 PUFAs content of 53.42%, 10.3% higher than that of CRL. The K_m and V_{max} value of HPHSM-C3@CRL was 42.2% lower and 63.5% higher than those of CRL, respectively. This present study suggested that hydrophobic microenvironment favored the activation and stability of lipase. The hierarchical pore contributed to the improved selectivity of immobilized lipase. This study provided an effective biocatalyst for the enzymatic enrichment of ω-3 PUFAs in glycerides, which also have potential in industrial applications and oil processing. In the future, the exploration on immobilization of CALA could be conducted to gain higher ω-3 PUFAs content in products.

CRediT authorship contribution statement

Zhe Dong: Writing – original draft, Methodology, Investigation, Formal analysis, Data curation, Conceptualization. **Jun Jin:** Writing – review & editing, Data curation. **Wei Wei:** Writing – review & editing.

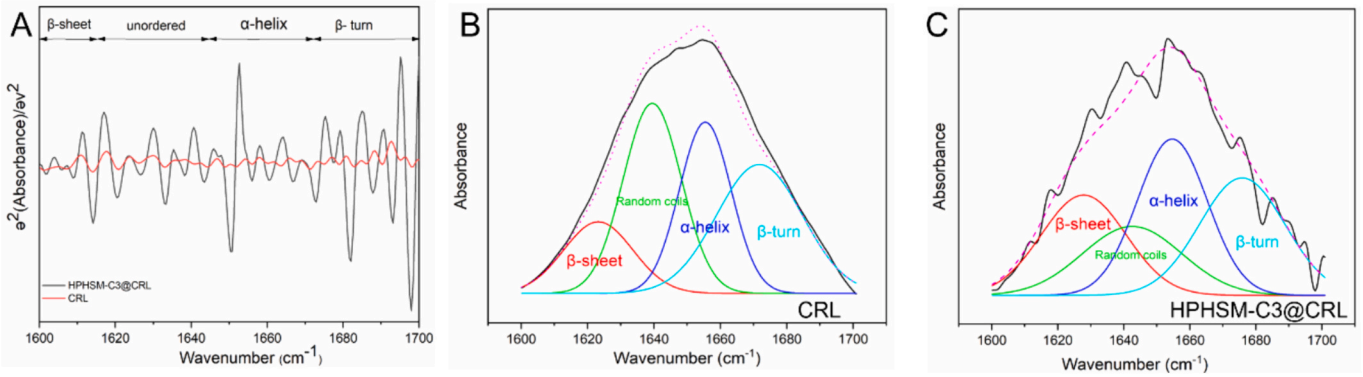

Fig. 5. (A) Second derivative of amide I band of CRL and HPHSM-C3@CRL; (B)CRL and (C) HPHSM-C3@CRL for secondary structural changes based on modeled multicomponent peak area by Gaussian multicomponent fitting.

Xiaosan Wang: Resources. **Gangcheng Wu:** Supervision, Funding acquisition. **Xingguo Wang:** Writing – review & editing, Methodology, Conceptualization. **Qingzhe Jin:** Writing – review & editing, Methodology, Conceptualization.

Declaration of competing interest

The authors declare no competing financial interest.

Data availability

Data will be made available on request.

Acknowledgments

This work was supported by National Key Research and Development Project of China (2021YFD2100303).

Appendix A. Supplementary data

Supplementary data to this article can be found online at https://doi.org/10.1016/j.fochx.2024.101434.

References

Adikwu Gowon, J., Roswanira Abdul, W., & Naji Arafat, M. (2021). Ternary biogenic silica/magnetite/graphene oxide composite for the hyperactivation of *candida rugosa* lipase in the esterification production of ethyl valerate. *Enzyme and Microbial Technology, 148*, 109807.

Aghaei, H., Ghavi, M., Hashemkhani, G., & Keshavarz, M. (2020). Utilization of two modified layered doubled hydroxides as supports for immobilization of *candida rugosa* lipase. *International Journal of Biological Macromolecules, 162*, 74–83.

Aghaei, H., Mohammadbagheri, Z., Hemasi, A., & Taghizadeh, A. (2022). Efficient hydrolysis of starch by α-amylase immobilized on cloisite 30b and modified forms of cloisite 30b by adsorption and covalent methods. *Food Chemistry, 373*, 131425.

Balasubramanian Ganesan, C. B., & Donald, J. M. (2014). Fortification of foods with omega-3 polyunsaturated fatty acids. *Critical Reviews in Food Science and Nutrition, 54* (1), 98–114.

Barriuso, J., Eugenia Vaquero, M., Prieto, A., & Jesus Martinez, M. (2016). Structural traits and catalytic versatility of the lipases from the *candida rugosa*-like family: A review. *Biotechnology Advances, 34*(5), 874–885.

Bispo, P., Batista, I., Bernardino, R. J., & Bandarra, N. M. (2014). Preparation of triacylglycerols rich in omega-3 fatty acids from sardine oil using a rhizomucor miehei lipase: Focus in the epa/dha ratio. *Applied Biochemistry and Biotechnology, 172* (4), 1866–1881.

Cao, Y. Y., Xia, Y. P., Gu, X. F., Han, L., Chen, Q. T., Zhi, G., & Zhang, D. (2020). Pei-crosslinked lipase on the surface of magnetic microspheres and its characteristics. *Colloids and Surfaces B: Biointerfaces, 189*, 110874.

Carlson, S. J., Fallon, E. M., Kalish, B. T., Gura, K. M., & Puder, M. (2013). The role of the ω-3 fatty acid dha in the human life cycle. *Journal of Parenteral and Enteral Nutrition, 37*(1), 15–22.

Chen, C., Karrar, E., Li, D., Zhao, P., Cheong, L.-Z., Wang, X., & Wei, W. (2023). Chemical mapping of milk fat globules using confocal raman microscopy: Comparison of different milk species and fat globule sizes. *International Dairy Journal, 146*, 105746.

Chen, Y., Cheong, L. Z., Zhao, J., Panpipat, W., Wang, Z., Li, Y., … Su, X. (2019). Lipase-catalyzed selective enrichment of omega-3 polyunsaturated fatty acids in acylglycerols of cod liver and linseed oils: Modeling the binding affinity of lipases and fatty acids. *International Journal of Biological Macromolecules, 123*, 261–268.

Chen, Y., Liu, K., Yang, Z., Chang, M., Wang, X., & Wang, X. (2023). Lipase-catalyzed two-step hydrolysis for concentration of acylglycerols rich in omega-3 polyunsaturated fatty acids. *Food Chemistry, 400*, 134115.

Dong, Z., Jin, J., Wei, W., Wu, G., Wang, X., & Jin, Q. (2024). Hyperactivation of lipase by oil-water interface in interfacial immobilization on hierarchical porous hollow silica microsphere: Dynamics, mechanism and application. *Food Bioscience, 58*, 103706.

Dong, Z., Liu, Z. S., Shi, J., Tang, H., Xiang, X., Huang, F. H., & Zheng, M. M. (2019). Carbon nanoparticle-stabilized Pickering emulsion as a sustainable and high-performance interfacial catalysis platform for enzymatic esterification/transesterification. *ACS Sustainable Chemistry & Engineering, 7*(8), 7619–7629.

Fletcher, P., Hamilton, R. F., Rhoderick, J. F., Postma, B., Buford, M., Pestka, J. J., & Holian, A. (2021). Therapeutic treatment of dietary docosahexaenoic acid for particle-induced pulmonary inflammation in balb/c mice. *Inflammation Research, 70* (3), 359–373.

Ghiaci, M., Aghaei, H., Soleimanian, S., & Sedaghat, M. E. (2009a). Enzyme immobilization part 1. Modified bentonite as a new and efficient support for immobilization of candida rugoso lipase. *Applied Clay Science, 43*(3), 289–295.

Ghiaci, M., Aghaei, H., Soleimanian, S., & Sedaghat, M. E. (2009b). Enzyme immobilization: Part 2. Immobilization of alkaline phosphatase on na-bentonite and modified bentonite. *Applied Clay Science, 43*(3–4), 308–316.

Giulio, P., Andr'es-Sanz, D., Marta, G., & Giuseppe, V. (2024). Deciphering the immobilization of lipases on hydrophobic wrinkled silica nanoparticles. *International Journal of Biological Macromolecules, 266*, 131022.

Hamidreza, A., Atefeh, Y., & Ameneh, T. (2021). Covalent immobilization of lipase from candida rugosa on epoxy-activated cloisite 30b as a new heterofunctional carrier and its application in the synthesis of banana flavor and production of biodiesel. *International Journal of Biological Macromolecules, 178*, 569–579.

He, J., Hong, B., Lu, R., Zhang, R., Fang, H., Huang, W., Bai, K., & Sun, J. (2020). Separation of saturated fatty acids from docosahexaenoic acid-rich algal oil by enzymatic ethanolysis in tandem with molecular distillation. *Food Science & Nutrition, 8*(5), 2234–2241.

He, Y., Li, J., Kodali, S., Balle, T., Chen, B., & Guo, Z. (2017). Liquid lipases for enzymatic concentration of n-3 polyunsaturated fatty acids in monoacylglycerols via ethanolysis: Catalytic specificity and parameterization. *Bioresource Technology, 224*, 445–456.

Hong, J., Lina, W., Duolao, W., Ni, Y., Chao, L., Min, W., Fan, W., Baibing, M., Fangyao, C., Wanru, J., Xi, L., Jiaxin, L., Yan, L., Jing, L., & Le, M. (2022). Omega-3 polyunsaturated fatty acid biomarkers and risk of type 2 diabetes, cardiovascular disease, cancer, and mortality. *Clinical Nutrition, 41*(8), 1798–1807.

Jiang, C., Chen, Y., Wang, Y. F., Li, C. M., Wang, X. S., Meng, Z., & Wang, X. G. (2022). Concentration of n-3 polyunsaturated fatty acid glycerides by lipase a-catalyzed selective methanolysis. *Food Bioscience, 46*, 101562.

Kahveci, D., & Xu, X. (2011). Repeated hydrolysis process is effective for enrichment of omega 3 polyunsaturated fatty acids in salmon oil by candida rugosa lipase. *Food Chemistry, 129*(4), 1552–1558.

Khozeymeh Nezhad, M., & Aghaei, H. (2021). Tosylated cloisite as a new heterofunctional carrier for covalent immobilization of lipase and its utilization for production of biodiesel from waste frying oil. *Renewable Energy, 164*, 876–888.

Liu, Y., & Dave, D. (2022). Recent progress on immobilization technology in enzymatic conversion of marine by-products to concentrated omega-3 fatty acids. *Green Chemistry, 24*, 1049–1066.

Liu, Z. Y., Huang, G., Guo, L., Li, X., & Xiao, J. (2022). Fabrication of lipase-loaded particles by coacervation with chitosan. *Food Chemistry, 385*, 132689.

Lu, T., & Chen, F. (2011). Multiwfn: A multifunctional wavefunction analyzer. *Journal of Computational Chemistry, 33*(5), 580–592.

Machado, N. B., Miguez, J. P., Bolina, I. C. A., Salviano, A. B., Gomes, R. A. B., Tavano, O. L., … Mendes, A. A. (2019). Preparation, functionalization and

characterization of rice husk silica for lipase immobilization via adsorption. *Enzyme and Microbial Technology, 128*, 9–21.
Miranda, K., Baeza-Jiménez, R., Noriega-Rodríguez, J. A., García, H. S., & Otero, C. (2013). Optimization of structured diacylglycerols production containing ω-3 fatty acids via enzyme-catalysed glycerolysis of fish oil. *European Food Research and Technology, 236*(3), 435–440.
Morales, A. H., Hero, J. S., Ledesma, A. E., Martínez, M. A., Navarro, M. C., Gómez, M. I., & Romero, C. M. (2023). Tuning surface interactions on $mgfe_2o_4$ nanoparticles to induce interfacial hyperactivation in *candida rugosa* lipase immobilization. *International Journal of Biological Macromolecules, 253*, 126615.
Moreno-Perez, S., Luna, P., Señorans, F. J., Guisan, J. M., & Fernandez-Lorente, G. (2015). Enzymatic synthesis of triacylglycerols of docosahexaenoic acid: Transesterification of its ethyl esters with glycerol. *Food Chemistry, 187*, 225–229.
Mortazavi, S., & Aghaei, H. (2020). Make proper surfaces for immobilization of enzymes: Immobilization of lipase and alpha-amylase on modified na-sepiolite. *International Journal of Biological Macromolecules, 164*, 1–12.
Mostafavi, M., Poor, M. B., Habibi, Z., Mohammadi, M., & Yousefi, M. (2024). Hyperactivation of lipases by immobilization on superhydrophobic graphene quantum dots inorganic hybrid nanoflower. *International Journal of Biological Macromolecules, 254*, 127817.
Nursyafiqah, E., Sheela, C., Fazira Ilyana Abdul, R., Joazaizulfazli, J., Nashi, W., & Roswanira Abdul, W. (2018). Characterization, optimization and stability studies on candida rugosa lipase supported on nanocellulose reinforced chitosan prepared from oil palm biomass. *International Journal of Biological Macromolecules, 114*, 306–316.
Okada, T., & Morrissey, M. T. (2007). Production of n−3 polyunsaturated fatty acid concentrate from sardine oil by lipase-catalyzed hydrolysis. *Food Chemistry, 103*(4), 1411–1419.
Parlett, C. M. A., Wilson, K., & Lee, A. F. (2013). Hierarchical porous materials: Catalytic applications. *Chemical Society Reviews, 42*(9), 3876–3893.
Rodrigues, R. C., Virgen-Ortíz, J. J., dos Santo, J. C. S., Berenguer-Murcia, A., Alcantara, A. R., Barbosa, O., … Fernandez-Lafuente, R. (2019). Immobilization of lipases on hydrophobic supports: Immobilization mechanism, advantages, problems, and solutions. *Biotechnology Advances, 37*(5), 746–770.
Sedaghat, M. E., Ghiaci, M., Aghaei, H., & Soleimanian-Zad, S. (2009). Enzyme immobilization. Part 4. Immobilization of alkaline phosphatase on na-sepiolite and modified sepiolite. *Applied Clay Science, 46*(2), 131–135.
Shahedi, M., Habibi, Z., Yousefi, M., Brask, J., & Mohammadi, M. (2021). Improvement of biodiesel production from palm oil by co-immobilization of thermomyces lanuginosa lipase and candida antarctica lipase b: Optimization using response surface methodology. *International Journal of Biological Macromolecules, 170*, 490–502.
Suladze, S., Cinar, S., Sperlich, B., & Winter, R. (2015). Pressure modulation of the enzymatic activity of phospholipase a2, a putative membrane-associated pressure sensor. *Journal of the American Chemical Society, 137*(39), 12588–12596.
Sun, Q., Aguila, B., Lan, P. C., & Ma, S. (2019). Tuning pore heterogeneity in covalent organic frameworks for enhanced enzyme accessibility and resistance against denaturants. *Advanced Materials, 31*(19), 1900008.
Sun, Q., Fu, C. W., Aguila, B., Perman, J., Wang, S., Huang, H. Y., … Ma, S. Q. (2018). Pore environment control and enhanced performance of enzymes infiltrated in covalent organic frameworks. *Journal of the American Chemical Society, 140*(3), 984–992.
Taiwo, O. A., Andrew, J. S., & Colin, J. B. (2014). Pancreatic lipase selectively hydrolyses dpa over epa and dha due to location of double bonds in the fatty acid rather than regioselectivity. *Food Chemistry, 160*, 61–66.
Vertegel, A. A., Siegel, R. W., & Dordick, J. S. (2004). Silica nanoparticle size influences the structure and enzymatic activity of adsorbed lysozyme. *Langmuir, 20*(16), 6800–6807.
Wang, S., Mo, L., Wu, B., Ma, C., & Wang, H. (2023). Effect of structural stability of lipase in acetonitrile on its catalytic activity in egcg esterification reaction: Ftir and md simulation. *International Journal of Biological Macromolecules, 255*, 128266.
Wu, J. H., Li, X. S., Zhao, Y., Gao, Q. A., Guo, L., & Feng, Y. Q. (2010). Titania coated magnetic mesoporous hollow silica microspheres: Fabrication and application to selective enrichment of phosphopeptides. *Chemical Communications, 46*(47), 9031–9033.
Yang, Z., Jin, W., Cheng, X., Dong, Z., Chang, M., & Wang, X. (2020). Enzymatic enrichment of n-3 polyunsaturated fatty acid glycerides by selective hydrolysis. *Food Chemistry, 346*(1), 128743.
Zhao, J., Ma, M., Yan, X., Wan, D., Zeng, Z., Yu, P., & Gong, D. (2022). Immobilization of lipase on beta-cyclodextrin grafted and aminopropyl-functionalized chitosan/fe_3o_4 magnetic nanocomposites: An innovative approach to fruity flavor esters esterification. *Food Chemistry, 366*, 130616.
Zhu, G., Zhu, X., Fan, Q., & Wan, X. (2011). Raman spectra of amino acids and their aqueous solutions. *Spectrochimica Acta. Part A, Molecular and Biomolecular Spectroscopy, 78*(3), 1187–1195.